Subwavelength light bending by metal slit structures

Tae-Woo Lee and Stephen K. Gray

Chemistry Division and Center for Nanoscale Materials, Argonne National Laboratory, Argonne, IL 60439
twlee@anl.gov, gray@tcg.anl.gov

Abstract: We discuss how light can be efficiently bent by nanoscale-width slit waveguides in metals. The discussion is based on accurate numerical solutions of Maxwell's equations. Our results, using a realistic model for silver at optical wavelengths, show that good right-angle bending transmission can be achieved for wavelengths $\lambda > 600$ nm. An approximate stop-band at lower wavelengths also occurs, which can be partly understood in terms of a dispersion curve analysis. The bending efficiency is shown to correlate with a focusing effect at the inner bend corner. Finally, we show that good bending transmission can even arise out of U-turn structures.

OCIS codes: (240.6680) Surface plasmons; (260.3910) Metals, optics of; (130.2790) Guided waves

References and Links

1. W. L. Barnes, A. Dereux, and T. W. Ebbesen, "Surface plasmon subwavelength optics," Nature (London) **424,** 824-830 (2003).
2. A. V. Zayats and I. I. Smolyaninov, "Near field photonics: surface plasmon polaritons and localized surface plasmons," J. Opt. A: Pure Appl. Opt. **5,** S16-S50 (2003).
3. T. W. Ebbesen, H. J. Lezec, H. F. Ghaemi, T. Thio, and P. Wolff, "Extraordinary optical transmission through sub-wavelength hole arrays," Nature (London) **391,** 667-669 (1998).
4. W. J. Fan, S. Zhang, B. Minhas, K. J. Malloy, and S. R. J. Brueck, "Enhanced infrared transmission through subwavelength coaxial metallic arrays," Phys. Rev. Lett. **94,** 033902 (2005).
5. S.-H. Chang, S. K. Gray, and G. C. Schatz, "Surface plasmon generation and light transmission by isolated nanoholes and arrays of nanoholes n thin metal films," Opt. Express **13,** 3150-3165 (2005), http://www.opticsexpress.org/abstract.cfm?URI=OPEX-13-8-3150.
6. S. A. Maier, P. G. Kik, H. A. Atwater, S. Meltzer, E. Harel, B. E. Koel, and A. A. G. Requicha, "Local detection of electromagnetic energy transport below the diffraction limit in metal nanoparticle plasmon waveguides," Nature Materials **2,** 229-232 (2003).
7. E. M. Hicks, S. Zou, G. C. Schatz, K. G. Spears, R. P. Van Duyne, L. Gunnarsson, T. Rindzevlclus, B. Kasemo, and M. Kall, "Controlling plasmon line shapes through diffractive coupling in linear arrays of cylindrical nanoparticles fabricated by electron beam lithography," Nano Letters **5,** 1065-1070 (2005).
8. K. Li, M. I. Stockman, and D. J. Bergman, "Self-similar chain of metal nanospheres as an efficient nanolens," Phys. Rev. Lett. **91,** 227402 (2003).
9. J. A. Porto, F. J. Garcia-Vidal, and J. B. Pendry, "Transmission resonances on metallic gratings with very narrow slits," Phys. Rev. Lett. **83,** 2845-2848(1999).
10. S. Collin, F. Pardo, R. Teissier, and J. L. Pellouard, "Strong discontinuities in complex photonic band structure of transmission metallic gratings," Phys. Rev. B **63,** 033107 (2001).
11. J. Bravo-Abad, L. Martin-Moreno, and F. J. Garcia-Vidal, "Transmission properties of a single metallic slit: From the subwavelength regime to the geometric-optics limit," Phys. Rev. E **69,** 026601 (2004).
12. Y. Xie, A. R. Zakharian, J. V. Moloney, and M. Mansuripur, "Transmission of light through slit apertures in metal films," Opt. Express **12,** 6106-6121 (2004), http://www.opticsexpress.org/abstract.cfm?URI=OPEX-12-25-6106.
13. D.-K. Qing and G. Chen, "Nanoscale optical waveguides with negative dielectric claddings," Phys. Rev. B **71,** 153107 (2005).
14. S.-Y. Lin, E. Chow, V. Hietala, P. R. Villeneuve, J. D. Joannopoulos, "Experimental demonstration of guiding and bending of electromagnetic waves in a photonic crystal," Science **282,** 274-276 (1998).
15. R. L. Espinola, R. U. Ahmad, F. Pizzuto, M. J. Steel, and R. M. Osgood, Jr., "A study of high-index-contrast 90 degree waveguide bend structures," Opt. Express **8**, 517-528 (2001), http://www.opticsexpress.org/abstract.cfm?URI=OPEX-8-9-517.
16. G. Veronis and S. Fan, "Bends and splitters in metal-dielectric-metal subwavelength plasmonic waveguides," Appl. Phys. Lett. **87**, 131102 (2005).

#9089 - $15.00 USD Received 10 October 2005; revised 9 November 2005; accepted 9 November 2005

17. L. Liu, Z. Han, and S. He, "Novel surface plasmon waveguide for high integration," Opt. Express **13**, 6645-6650 (2005), http://www.opticsexpress.org/abstract.cfm?URI=OPEX-13-17-6645.
18. A. Taflove and S. C. Hagness, *Computational Electrodynamics: The Finite-Difference Time-Domain Method*, 2nd ed. (Artech House, Boston, 2000).
19. P. B. Johnson and R. W. Christy, "Optical constants of the noble metals," Phys. Rev. B **6,** 4370-4379 (1972).
20. S. K. Gray and T. Kupka, "Propagation of light in metallic nanowire arrays: Finite-difference time-domain results for silver cylinders," Phys. Rev. B **68,** 045415 (2003).
21. T. O. Körner and W. Fichtner, "Auxiliary differential equation: efficient implementation in the finite-difference time-domain method," Opt. Lett. **22,** 1586 (1997).
22. N. Marcuvitz, *Waveguide Handbook* (Peter Peregrinus Ltd., London, 1986). First published in *MIT Radiation Laboratory Series* (McGraw-Hill, New York, 1951).
23. J. J. Campbell and W. R. Jones, "Symmetrically truncated right-angle corners in parallel plate and rectangular wavegudies," IEEE Trans. Microwave Theory and Tech., **MTT-16,** 517 (1968).
24. C. A. Balanis, *Advanced Engineering Electromagnetics* (John Wiley & Sons, New York, 1989).
25. E. T. Arakawa, M. W. Williams, R. N. Hamm, and R. H. Ritchie, "Effect of damping on surface plasmon dispersion," Phys. Rev. Lett. **31**, 1127-1129 (1973).
26. P. M. Morse and H. Feshbach, *Methods of Theoretical Physics*, Part II, 1250-1251 (McGraw-Hill, New York, 1953)
27. F. J. Gracia-Vidal, H. J. Lezec, T. W. Ebbesen, and L. Martin-Moreno, "Multiple paths to enhance optical transmission through a single subwavelength silit," Phys. Rev. Lett. **90,** 213901 (2003).
28. S. S. Akarca-Biyikli, I. Bulu, and E. Ozbay, "Enhanced transmission of microwave radiation in one-dimensional metallic gratings with subwavelength aperture," Appl. Phys. Lett **85,** 1098 (2004).

1. Introduction

Understanding how to confine and manipulate light on a subwavelength scale is central to advancing nanoscale-based optics, spectroscopy and optoelectronics. Nanostructured metallic systems, typically composed of silver or gold, are often studied because they can exhibit surface plasmons (SPs) at optical wavelengths [1, 2]. SPs are electromagnetic surface waves corresponding to collective electronic excitations near the metal surface. By coupling light into SPs one can attempt to confine, concentrate and propagate electromagnetic energy in a subwavelength limit. Interesting results with nanoscale holes in metal films [3-5] and arrays of metal nanoparticles [6-8] have been obtained. There can be other useful phenomena, not requiring SPs, that lead to subwavelength confinement and transmittance of light. For example, subwavelength slits can exhibit waveguide modes, including transverse electromagnetic (TEM) modes that exist for any slit width [9-13]. Redirecting or bending propagating light at subwavelength scales is also a key element for realizing high density integrated optics based on nanoscale-based photonic components. Photonic bandgap structures [14], as well as high dielectric resonant structures [15], can bend light. However, the corresponding system dimensions are on the order of the wavelength or larger, making them less appropriate for nanoscale optical elements.

It is natural to inquire if metal slit structures, or 3-D analogs such as trenches in thin metal films might be used to bend light on subwavelength scales. Indeed, recent finite-difference frequency-domain calculations by Veronis and Fan [16] show that very efficient right-angle bending and splitting is possible for d = 50-100 nm slit structures in silver with wavelengths $\lambda >> d$. Liu, Han and He [17], using finite-difference time-domain (FDTD) [18] calculations, showed that 50 nm wide trenches in 200 nm thick silver films could also bend λ = 632.8 nm light reasonably well, and that rounding off the bend can improve the efficiency. Our work is most directly related to these two studies. We first carry out FDTD calculations on right-angle bend slit structures similar to those of Veronis and Fan [16]. Our results fully confirm their conclusions. We then go on to show how the plasmonic structure of real silver can lead to stop-band behavior, and analyze the origins of this behavior by computing a metal-air-metal waveguide dispersion curve. Consistent with Liu, Han and He [17], we find that smoothing the bend can enhance the transmission. Furthermore, we find that only the outer portion of the bend need be rounded to obtain high bending transmittance, allowing for a tighter bend region. By inspection of time sequences of our FDTD results, we find that a sharp inner bend

#9089 - $15.00 USD Received 10 October 2005; revised 9 November 2005; accepted 9 November 2005

leads to a focusing effect that can be correlated with efficient bending transmission. Finally, we show that a U-turn slit structure can also lead to remarkably good bending transmission.

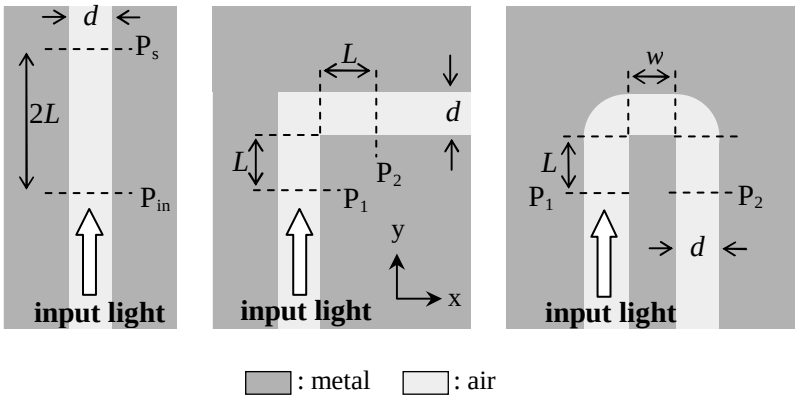

Fig. 1. Schematic diagrams of the systems studied: straight , right-angle bend, and U-turn slit structures.

Section 2 below discusses the details of our numerical calculations, Sec. 3 presents our right-angle bend results and Sec. 3 presents the U-turn results. Concluding remarks are in Sec. 4.

2. Computational details

We propagate grid representations of the electromagnetic fields, **E** and **H**, in the metallic structures of Fig. 1. These structures are two-dimensional, since invariance with respect to *z* out of the *x*-*y* plane is assumed, but they could be realized experimentally with appropriately thick metal slabs. Our focus is on transverse magnetic (TM) modes, defined relative to the *x*-*y* propagation plane. These modes involve propagation of two electric field components, $E_x(x,y,t)$, $E_y(x,y,t)$, and the transverse magnetic field component, $H_z(x,y,t)$, in time, *t*. The other modes, TE modes, have non-zero cut-off frequencies and cannot be supported in our subdiffraction structures. If the metal is a perfect electrical conductor (PEC), the fields are propagated, with the standard FDTD updating scheme [18], coupled with setting E_x and E_y to be zero in metallic regions. We also carry out calculations treating the metal as silver with a Drude plus two-pole Lorentzian form for its dielectric constant,

$$\varepsilon_M(\omega) = \varepsilon_\infty - \frac{\omega_D^2}{\omega^2 + i\gamma_D\omega} - \sum_{m=1}^{2} \frac{g_{L_m}\,\omega_{L_m}^2\,\Delta\varepsilon}{\omega^2 - \omega_{L_m}^2 + i2\gamma_{L_m}\omega} \quad . \tag{1}$$

We find ε_∞ = 2.3646, ω_D = 8.7377 eV, γ_D = 0.07489 eV, $\Delta\varepsilon$ = 1.1831, g_{L_1} = 0.2663, ω_{L_1} = 4.3802 eV, γ_{L_1} = 0.28 eV, g_{L_2} = 0.7337, ω_{L_2} = 5.183 eV, γ_{L_2} = 0.5482 eV provide a good description of empirical dielectric constant data for silver [19] over the λ = 250 nm – 1000 nm range of interest, which includes the interband region near 325 nm, as shown in Fig. 2(a). Eq. (1) thus adequately describes the silver absorption loss, related to Im[ε_M], and frequency (or wavelength) dispersion.

FDTD calculations consistent with Eq. (1) are accomplished with an auxiliary differential equation (ADE) approach [18]. In our case, this involves propagation of Drude ($\mathbf{P}_D$) and Lorentzian ($\mathbf{P}_{L1}$, $\mathbf{P}_{L2}$) polarization vectors. We infer $\mathbf{P}_D$ from a current vector ADE method [20]; $\mathbf{P}_{L1}$, and $\mathbf{P}_{L2}$ are inferred as in Ref. [21]. Instead of updating **E**, it is convenient to update the electric flux density, **D**. To update **H** we still need **E**, which is obtained from,

#9089 - $15.00 USD Received 10 October 2005; revised 9 November 2005; accepted 9 November 2005

$$\mathbf{E}(t) = \frac{\mathbf{D}(t) - \mathbf{P}_D(t) - \sum_{m=1}^{2} \mathbf{P}_{L_m}(t)}{\varepsilon_0 \varepsilon_\infty} \tag{2}$$

Field components approaching the outer edges of the grid are absorbed with uniaxial, perfectly matched layers [18]. A 2 nm grid spacing is used for both the *x* and *y* grids. The full grid is 500 nm x 2200 nm for the straight structure and 2000 nm x 2200 nm for the bent structure.

Waveguide modes are excited with a soft source [18], which involves updating H_z along a horizontal line within a waveguide section near the bottom end using a sinusoidal pulse. Source amplitude is uniform along the source line. The sinusoid is enveloped in time by a Blackman-Harris window, generating a pulse with a range of frequencies. The source spectral content covers the relevant λ = 250 nm - 1000 nm range. Fourier transforms of the time-dependent fields yield the spectral domain information. Incident power, P_{in}, and transmitted powers, P_s and P_2, are calculated by integrating the normal component of the Poynting vector along the dashed lines in Fig. 1. A power P_1 for the bent structure, based on the same line as P_{in}, is also indicated. The lines for P_{in} and P_1 are 1.5 μm above the source line, allowing enough space for guided modes to form above them. For the right-angle bend (center, Fig. 1), the bending region is introduced L = 100 nm above the P_1 line. The same distance L also separates the P_2 line from the bending region. For the U-turn (far right, Fig. 1), the bending region starts L = 100 nm above P_1. A horizontal, straight waveguide with length w = 100 nm connects it to a second right-angle bend, leading downward. The P_2 line is set at a distance L below the second bend, as indicated. Using the same source excitation, the straight waveguide transmittance is $T_s = P_s/P_{in}$ and the bend and U-turn transmittance is $T_b = P_2/P_{in}$.

3. Right-angle bend

Figure 2(b) shows the bending transmittance, T_b, treating the metal as a PEC, for slit widths *d*

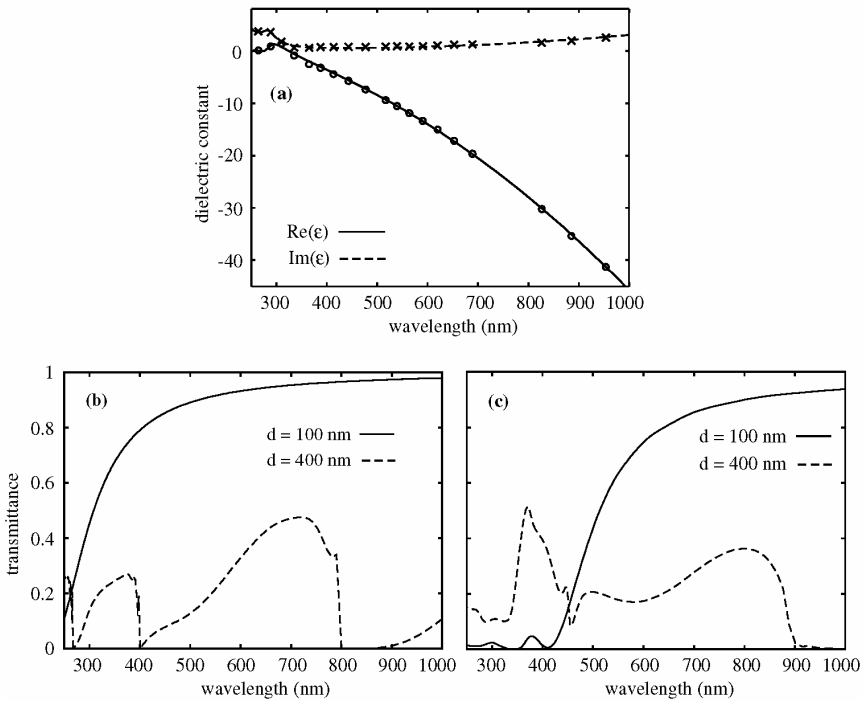

Fig. 2. (a) The Ag dielectric constant, with the solid curves being our Drude-Lorentz model and the symbols being empirical data [19]. (b) Bending transmittance, T_b, for a PEC right-angle bend with two different slit widths, *d*. (c) The same as (b) except now with the Drude-Lorentz Ag model.

#9089 - $15.00 USD Received 10 October 2005; revised 9 November 2005; accepted 9 November 2005

= 100 nm and 400 nm. For d = 100 nm, T_b approaches unity with increasing λ. With $\lambda > 5\ d$, we have $T_b > 0.9$. This behavior is not entirely unexpected: older, equivalent circuit models [22] and more rigorous calculations [23] developed in the context of microwave theory show, in the quasistatic limit, that T_b should indeed approach unity for a PEC. Fig. 2(c), however, shows that when Eq. (1), a realistic (absorbing and dispersive) model for silver is used, T_b can still be high. Relative to the d = 100 nm PEC results, T_b significantly lower for λ < 500 nm, but high transmittance is rapidly recovered at longer wavelengths: $T_b > 0.9$ for λ > 800 nm. These d = 100 nm results are similar to those of Veronis and Fan [16]. The wider, d = 400 nm, slit results in Figs. 2(b) and 2(c) exhibit considerably less transmittance and also show more structure than the d = 100 nm results. In the PEC case [Fig. 2(b)], the abrupt minima can be associated with cut-off wavelengths of various waveguide modes that correlate well with the cut-off wavelengths of the straight slit TM_m modes, which are given by $\lambda_c = 2d/m$, m = 1, 2, As λ increases in Fig. 2(b), the m = 3, 2, and 1 modes become allowed at approximately 267, 400 and 800 nm. Note that while the source excitation profile corresponds to m = 0 (uniform H_z with respect to x), the bend allows coupling to higher order modes. Since the dimensions of a PEC waveguide are scalable with wavelength, the d = 400 nm slit will exhibit high transmittance when λ is increased further. The d = 400 nm results for silver, Fig. 2(c), do not correlate as well with the simple expectations owing to wavelength dependent losses.

Non-unit T_b can arise from two features: (i) "reflection," which we take to be the energy flow returning back to the input terminal due to the discontinuity of bending structure and (ii) absorption loss in the case of silver. One thus expects that rounding the outer edge of the bend should reduce reflection and improve bending transmittance, which would also be consistent with the metal trench calculations of Liu, Han and He [17]. Specifically, we modified d = 100 nm case bent structure of Fig. 1 by rounding the outer corner with a quarter circle of radius 100 nm. Unlike Ref. [17], however, the sharp inner corner is retained. This allows for a more compact bending region. Figure 3 shows transmittance (solid curve) for this slightly rounded bend with our realistic silver model. For reference we also show transmittance for the straight slit case (Fig. 1, left) in silver as a dashed curve. For λ < 350 nm the transmittance of both structures is relatively small, with the rounded bend showing the least transmittance over this range. However, as λ increases, transmittance from both structures increases and bending loss diminishes. Remarkably, we find $T_b > 0.95$ for $\lambda > 700$ nm. Relative to the square outer corner case [Fig. 2(c)], a large improvement in transmittance is seen in Fig. 3(a) for 400 nm $< \lambda <$ 600 nm. This implies that reflection from the outer bend region is much more significant when low transmittance occurs. The discontinuity introduced by sharp inner corner does not have a detrimental effect on T_b. Structures with rounded inner and outer corners also reduce reflectance [17]. However, these latter structures can have longer optical paths in the bending region and thus exhibit more absorption loss.

The transmittance in Fig. 3 for λ < 350 nm represents an approximate stop-band,

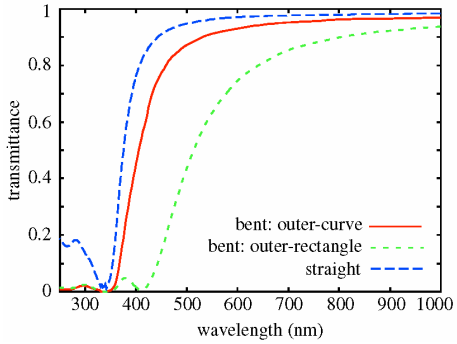

Fig. 3. Transmittance results for a rounded outer bend wall (red solid curve) are compared with the corresponding transmittance through a straight slit (blue long-dashed curve) and rectangle outer wall (green short-dashed curve.

#9089 - $15.00 USD Received 10 October 2005; revised 9 November 2005; accepted 9 November 2005

introduced by the more complex dielectric constant behavior of silver, as we now show. Since

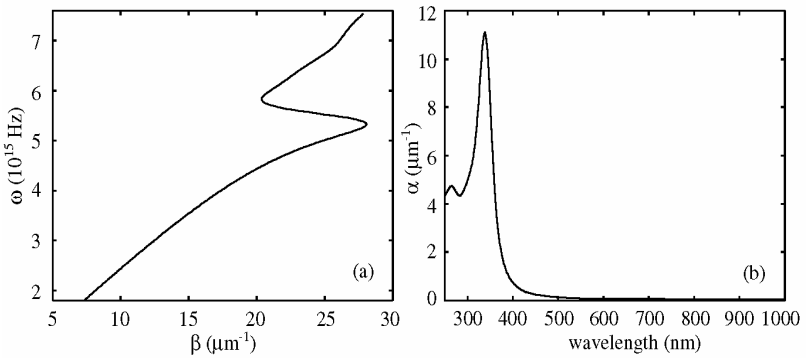

Fig. 4. (a) Dispersion relation of the lowest, even mode for a d = 100 nm straight slit in silver, with being the real part of the propagation constant. (b) The extinctions coefficient of as a function of wavelength, the imaginary part of propagation constant.

there are parallels between T_s and T_b in Fig. 3, we analyze the more analytically tractable, straight slit case to learn more about the approximate stop-band behavior. We obtained waveguide modes by numerically solving the transcendental equation for the propagation coefficient of a symmetric slab waveguide [24] composed of a central, 100 nm thick slab of air surrounded by silver with complex dielectric constant Eq. (1). The propagation coefficient is thus complex and, with our axis convention (Fig. 1), corresponds to the y-component of the wave vector, $k_y = \beta + i\alpha$; β, α = real numbers. The dispersion relations for the various modes are somewhat involved, and for clarity Fig. 4 displays just the dispersion relation for the lowest order even mode, TM_0. This mode naturally shares features in common with the air/metal interface SP dispersion relation [1, 2]. Fig. 4(a) shows that the $\omega \approx 5.5 \times 10^{15}$ - 6×10^{15} Hz region (λ = 340-310 nm) of $\omega(\beta)$ exhibits "backbending," i.e. has $d\omega/d\beta < 0$, a feature also seen in SP dispersion relations when damping is allowed for [25]. (The nature of wave packets composed of frequencies in the backbending region is an interesting, separate issue that we are currently exploring.) Figure 4(b) shows that the decay constant is particularly large in the backbending region, so that absorption loss is the origin of the effective stop-band behavior seen in Fig. 3. Indeed, we find $\exp[-4\alpha(\omega)L]$ is very close to the straight slit transmission of Fig. 3. The bent slit transmittance in silver for this spectral region is even smaller than the straight-slit case and the approximate stop-band behavior extends outside the 340-310 nm spectral range, owing to reflection and higher-order mode coupling effects.

The transmittance discussed so far concerns a nanoscale region, with dimensions on the order of $2L \times 2L$ = 200 nm x 200 nm (Fig. 1). However, it is also natural to ask how long a signal can propagate either before or after being bent on the nanoscale. The intensity of a mode will decay to $1/e$ of its value after a distance $1/(2\alpha)$; $1/(2\alpha) \approx 12$ mm for the TM_0 mode in Fig. 4 at λ = 1000 nm. Thus one can propagate significantly larger distances into and out of bends in silver.

We examine snapshots of the electric field intensity as light is efficiently bent through a slit structure. Figure 5 displays the steady state intensity for λ = 1000 nm for times t, $t + 0.4 \times 10^{-15}$ s, and $t + 0.8 \times 10^{-15}$ s. The steady state is obtained with a pure sinusoidal, as opposed to pulsed, source excitation at the wavelength of interest**,** and propagating to times t such that transient wavelengths are absent. The results in Fig. 5 correspond to the realistic silver model with a rounded outer bend wall, although similar results are obtained with use of a PEC and/or a right-angled outer bend wall. One sees light intensity building near the inner corner and effectively focusing the incoming light from the lower portion of the structure and transmitting it to the upper portion. In the quasistatic limit of a PEC bend, this focusing effect is represented by a singularity at the corner [26]. When λ is decreased, or d is increased, the portion of energy flow focused at the inner corner becomes smaller. A larger portion of the

#9089 - $15.00 USD Received 10 October 2005; revised 9 November 2005; accepted 9 November 2005

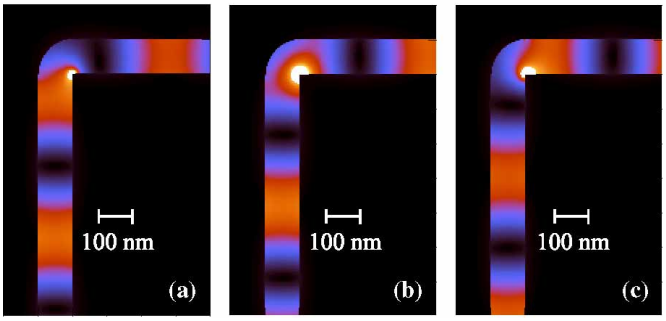

Fig. 5. The square of the magnitude of the (real) electric field for times (a) t, (b) $t + 0.4 \times 10^{-15}$ s, and (c) $t + 0.8 \times 10^{-15}$ s, where t is a time such that the steady state limit has been achieved (see text).

light interacts with the outer corner region, resulting in higher reflection and reduced transmittance. Absorption loss for silver, not present in the PEC case, also contributes to the reduced transmittance at lower wavelengths. The absorption loss is also diminished for longer wavelength as silver approaches the PEC limit. The focusing effect also explains how the shape of the outer corner is not important at wavelengths corresponding to high transmittance, as discussed earlier in relation to Fig 3.

4. U-turn

Figure 6 displays the bending transmittance obtained for the U-turn slit structure (Fig. 1, right) with our Drude-Lorentz silver model. As with the right-angle bend case discussed in Sec. 3, the transmittance can be remarkably high, better than 90%, in the $\lambda >> d$ limit. (We do not display transmittance for $\lambda < 400$ nm because in this limit the source, placed in the left channel of the U-turn, leads to waves that couple into the right channel prior to reaching the bend. This is because a realistic metal becomes more dielectric-like in the limit of small wavelengths, allowing for waves to pass more through it.) The inner corner focusing effect identified in Sec. 3 also exists in this case. Figure 7 gives a snapshot, and movie (formatted with the Cinepak AVI codec), illustrating the effect. The figure was generated using a soft source tuned to $\lambda = 1000$ nm in the lower part of the left channel. It also illustrates clearly the excellent bending transmission.

5. Concluding remarks

Summarizing, a variety of calculations were undertaken to probe how right-angle bends and U-turns in nanoscale slit structures in metals can transmit light. Perfect electrical conductors (PECs) exhibit excellent bending transmittance for wavelengths long compared to the slit width, a result that is not unexpected from microwave theory and the fact that PEC problems

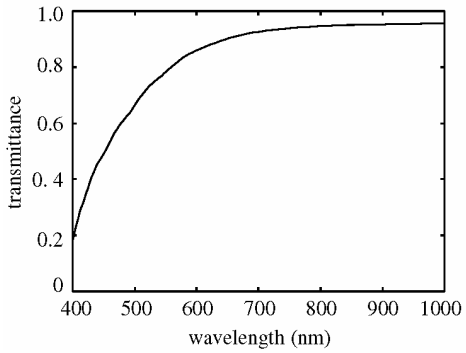

Fig. 6. Transmittance results for U-turn. The outer wall is rounded as in the right-side figure of Fig. 1.

#9089 - $15.00 USD Received 10 October 2005; revised 9 November 2005; accepted 9 November 2005

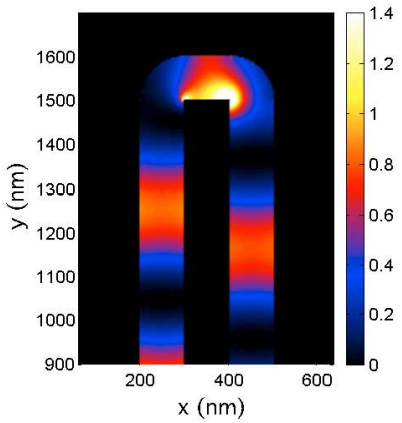

Fig. 7. (1.5MB, video for wave propagation) The square of the magnitude of the (real) electric field propagating in a U-turn waveguide.

scale to any system size.

Since excellent bending transmission occurs for PEC bends which do not support surface plasmons (SPs), it would be incorrect to attribute the phenomenon discussed here to SPs. However when a realistic silver model, including dispersion, absorption and supporting SPs at the optical wavelengths of interest, is studied, good transmittance is still found. Rounding off the bend outer edge leads to better transmittance. Our right-angle bend slit results are consistent with those of Veronis and Fan [16], and the rounding result is similar in spirit to that of Liu, Han and He [17]. Moreover, a richer transmittance structure than with PECs is found for right-angle bends at moderate wavelengths compared to the slit width, involving approximate stop-bands. We were able to understand this behavior with a dispersion curve analysis. The bending efficiency in these systems was also correlated with a focusing effect at the inner corners.

The features discussed here should be experimentally observable. Current photolithography and material processing techniques, such as lift-off etching followed by metal deposition, could be used to fabricate nanoscale bending patterns with considerably high metal walls, or deep trenches, closely approximating the bending structures we modeled. Coupling external light into and out of the structures must also be considered. Gratings surrounding the slit openings [27, 28] could enhance the coupling efficiency. Another obvious approach would be to use larger slit openings, which narrow down to the intended slit width. The remarkable physical properties of nanoscale bent slits in metals could open up exciting new avenues for nanophotonics research and nanoscale device applications.

Acknowledgments

This work was supported by the U. S. Department of Energy, Office of Basic Energy Sciences, Division of Chemical Sciences, Geosciences, and Biosciences under DOE contract W-31-109-ENG-38. We are grateful to L. E. Ocula and L. Queue for helpful comments.

#9089 - $15.00 USD Received 10 October 2005; revised 9 November 2005; accepted 9 November 2005